AIAA JOURNAL
Vol. 33, No. 12, December 1995

# Compressibility Effects and Mixing Enhancement in Turbulent Free Shear Flows

Tong-Miin Liou,* Wan-Yih Lien,† and Po-Wen Hwang†
*National Tsing Hua University, Hsinchu 30043, Taiwan, Republic of China*

**Computational simulations have been performed to study compressible, spatially developing turbulent free shear layers with various velocity regimes—subsonic/subsonic, supersonic/subsonic, and supersonic/supersonic—for convective Mach numbers in the range of 0.14–1.28. The numerical code used the finite volume technique and a modified Godunov's scheme. The computed results for the supersonic/subsonic case are first compared with experimental axial mean-velocity profiles, vorticity thickness, and turbulence parameters. Mixing layers with various velocity regimes are then calculated to investigate compressibility effects on the evolution of large-scale structures through the flow visualization of the vorticity field, growth rate of the vorticity thickness, and vorticity dynamics analysis. Various forcing frequencies are applied at the inflow boundary to examine mixing enhancement for free shear layers with higher convective Mach numbers. It is found for the first time that the growth rate of supersonic/supersonic free shear layers increases markedly when the forced layers move up and down with time instead of forming vortex roll-up and pairing.**

## Nomenclature

$a$ = speed of sound, m/s
$e$ = total energy per unit volume, J/m$^3$
$F$ = convective flux vector in $x$ direction
$f_0$ = fundamental frequency, 1/s
$f_1$ = first subharmonic frequency, $f_0/2$, 1/s
$f_2$ = second subharmonic frequency, $f_0/3$, 1/s
$G$ = convective flux vector in $y$ direction
$L$ = axial length of computational domain, m
$M$ = Mach number
$M_c$ = convective Mach number, $(\bar{u}_1 - u_c)/a_1$
$p$ = pressure, N/m$^2$
$Q$ = conservation variables vector
$t$ = time coordinate, s
$t^*$ = nondimensionalized time, $t/(L/\bar{u}_a)$
$u$ = velocity in $x$ direction, m/s
$u^*$ = nondimensionalized velocity, $(\bar{u} - \bar{u}_2)/(\bar{u}_1 - \bar{u}_2)$
$\bar{u}_a$ = average inlet velocity, $(\bar{u}_1 + \bar{u}_2)/2$, m/s
$u_c$ = convective velocity, $(a_1\bar{u}_2 + a_2\bar{u}_1)/(a_1 + a_2)$, m/s
$v$ = velocity in $y$ direction, m/s
$x$ = longitudinal coordinate, cm
$y$ = transverse coordinate, cm
$y_0$ = location where $\bar{u} = (\bar{u}_1 + \bar{u}_2)/2$, cm
$y^*$ = $(y - y_0)/\delta_\omega$
$\gamma$ = specific heats ratio
$\delta_\omega$ = vorticity thickness, $(\bar{u}_1 + \bar{u}_2)/(\partial\bar{u}/\partial y)_{\max}$, cm
$\delta'_\omega$ = growth rate of vorticity thickness, $d\delta_\omega/dx$
$\theta$ = momentum thickness, cm
$\rho$ = density, kg/m$^3$
$\sigma_u$ = streamwise turbulence intensity
$\sigma_v$ = lateral turbulence intensity

*Subscripts*

$i$ = incompressible
1 = top stream; Fig. 1
2 = bottom stream; Fig. 1

*Superscripts*

$'$ = turbulent fluctuation value of variable
$-$ = time-averaged value

## Introduction

THE spatially developing shear layer generated by turbulent mixing of two coflowing fluid streams, as shown schematically in Fig. 1, has been one of the most active areas of research in fluid mechanics and is encountered in many engineering applications. The large quasi-two-dimensional coherent vortical structures in subsonic turbulent free shear flows were first observed by experimental investigations,[1,2] which drastically altered researchers' perceptions of the mixing process in these flows. In the recent development of efficient supersonic combustion ramjet (scramjet) engines and advanced aerospace propulsion systems, there is renewed interest in the study of supersonic turbulent mixing layers. Most current concepts relevant to the scramjet engines employ the mixing-limited heat release, which depends on the rate of mass and momentum transfer across the fuel-air shear layer and hence can be described using the shear layer growth rate. Unfortunately, experiments[3–5] showed that the growth rate of the mixing layer in two supersonic streams is considerably smaller than that in two subsonic streams. It is therefore important to find methods or mechanisms to enhance the mixing rate between the two coflowing supersonic streams. Furthermore, even if only one of the streams in a shear layer is supersonic, experiments[6,7] still reveal that the growth rate decreases with increasing convective Mach number ($M_c$). The term $M_c$ is defined as $M_c = (\bar{u}_1 - u_c)/a_1$, where $u_c = (a_1\bar{u}_2 + a_2\bar{u}_1)/(a_1 + a_2)$[6,7] and $M_c$ is a parameter characterizing the compressibility effects in shear flows.[3,5] Most experiments on compressible shear layers were limited to the mean flow measurements and the compressibility effects on the shear layer growth rate.[3–5] There are few experiments[6,7]

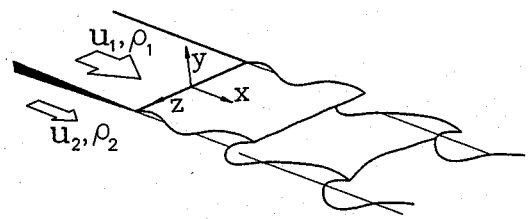


**Fig. 1 Schematic illustration of flow configuration and geometry in a mixing layer.**

Received Jan. 5, 1995; revision received June 26, 1995; accepted for publication July 12, 1995. 

*Professor, Department of Power Mechanical Engineering.
†Graduate Student, Department of Power Mechanical Engineering.

providing, in addition to the mean flow data and growth rate, the turbulence information for validating the computational schemes. Recently, Lele[8] has reviewed the features of the turbulent state that depend on compressibility and gave a good overview on compressible mixing layers.

Computationally, a fair number of numerical studies on the spatially developing mixing layers have been carried out using two subsonic[9–11] or two supersonic[12–14] parallel streams of gas. In contrast, the computation of mixing layers formed by a supersonic and a subsonic stream has received limited attention to date; however, this type of flow regime is often encountered in the practical ramjet combustor and ejector and is associated with the noise problem caused by a supersonic jet discharging into a subsonic stream. Farouk et al.[12] used the flux-corrected transport algorithm mainly to study the mixing and stability in a shear flow of two supersonic streams; partly, they reported the results of a limited computation on a shear layer resulting from the mixing of a supersonic and a subsonic stream. Their results regarding the supersonic-subsonic interaction were only presented in terms of the flow visualization of the mixing ratio and the spectra of pressure fluctuations, without quantitatively comparing them with available experimental measurements. This fact provides one of the motivations for the present study.

This paper attempts to develop a numerical algorithm to study the large vortical structures and their evolution in the spatially developing mixing layers between two fluid streams at three types of velocity regimes: subsonic/subsonic, supersonic/subsonic, and supersonic/supersonic. The present numerical method solves the governing equations directly using a modified Godunov's scheme without subgrid-scale (SGS) turbulence models; consequently, the complexity of empirical turbulence models, especially those with compressibility correction terms, can be avoided. Liou et al.[15] have recently demonstrated the applicability of this numerical method to the study of subsonic turbulent nonreacting and reacting flows in a coaxial sudden-expansion combustion chamber with gaseous fuel radially injected from the porous wall. The present work extends the calculations to the spatially developing turbulent free shear layers of various velocity regimes and assesses the numerical algorithm by comparing the calculated results of the supersonic/subsonic velocity regime with existing experimental data.[6,7] In addition, the effects of compressibility on the large coherent structures and growth rate of the vorticity thickness are discussed. The other major objective of this paper is to devise techniques for enhancing the mixing in supersonic shear layers whose growth rates are significantly less than those of incompressible shear layers.

## Governing Equations and Numerical Algorithm

Experiments[1,2,16] have confirmed that the evolution of mixing layers at low $M_c$ is mainly characterized by large, organized two-dimensional vortices and their pairing. To examine whether three-dimensional obliquity prevails for high $M_c$ flows, Papamoschou[17] showed experimentally no obvious evidence that the large structures are obliquely oriented at high $M_c$. Experimental results of Clemens and Mungal[18] showed that the supersonic mixing layer, when driven to a low $M_c$ of 0.28, behaves as an incompressible layer with characteristic two-dimensional organized structures. As $M_c$ increases to 0.62 and 0.79, the mixing layer becomes three dimensional. Sandham and Reynolds[19,20] used both linear theory and numerical simulations to show that three-dimensional structure may occur for $M_c$ above 0.6. Although the turbulent mixing layer at high $M_c$ would be three dimensional, two-dimensional numerical simulations have been shown to capture satisfactorily the major features of subsonic mixing layers[9–11,21] and supersonic mixing layers,[12–14] especially in predicting the growth rate of a mixing layer. The major objective of the present simulations is to examine the effects of compressibility on the growth rate and to devise techniques for enhancing the mixing in supersonic shear layers. Therefore, it would not be unrealistic to perform two-dimensional simulations. In addition, the basic vortex dynamics in a shear layer is essentially inviscid,[9,30] which suggests that the present simulations can be formulated using two-dimensional Euler's equations.

### Governing Equations

The compressible Euler equations in two-dimensional Cartesian coordinates without body forces and external heat addition can be written as

$$\frac{\partial Q}{\partial t} + \frac{\partial F}{\partial x} + \frac{\partial G}{\partial y} = 0 \tag{1}$$

where $Q$, $F$, and $G$ are vectors given by

$$Q = \begin{bmatrix} \rho \\ \rho u \\ \rho v \\ e \end{bmatrix}, \quad F = \begin{bmatrix} \rho u \\ \rho u^2 + p \\ \rho uv \\ (e+p)u \end{bmatrix}, \quad G = \begin{bmatrix} \rho v \\ \rho uv \\ \rho v^2 + p \\ (e+p)v \end{bmatrix} \tag{2}$$

The equations represent the conservation of mass, momentum, and total energy of inviscid fluid motion. For an ideal gas, the pressure is related to the equation of state

$$p = (\gamma - 1)[e - 0.5\rho(u^2 + v^2)] \tag{3}$$

### Numerical Algorithm

The code used the finite volume technique.[15] An explicit scheme was selected to resolve the time evolution of the large scales in turbulent flowfields. The vector $Q$ in Eq. (2) representing conservative variables was calculated at the center of each computational cell and the flux vectors $F$ and $G$ in Eq. (2) were calculated at the cell edges using Godunov's scheme.[22] The basic idea behind Godunov's scheme is to use the exact solution of the gasdynamic equations with piecewise initial states to construct the finite difference schemes. Godunov used the characteristic information so that the Riemann problem could be solved forward in time and then used the solution of the Riemann problem to calculate the numerical flux at the cell edges. The major disadvantage of Godunov's original scheme is the first-order spatial accuracy, which results in a relatively poor resolution of flow structures. To improve the order of spatial accuracy of Godunov's original scheme, in this work the piecewise initial states to the left and right of the cell edges were obtained by a second-order extrapolation. In addition, a limiting technique was applied to achieve numerical stability. Three benchmark test cases were given[23] to examine the accuracy of the present scheme, including a one-dimensional Riemann's shock tube problem at pressure ratio of 10, a one-dimensional two interacting blast waves problem at pressure ratios up to $10^5$, and a two-dimensional shock reflection problem. Comparison with the exact solutions demonstrated the robust stability of the present scheme with complicated wave developments and interactions. A detailed derivation of the modified Godunov's scheme and its improvement on the numerical accuracy were presented in the work of Liou et al.[23]

### Boundary and Initial Conditions

The primitive variables $(\rho, u, v, p)$ need to be specified at the boundaries of the finite computational domain because they are involved in the flux vectors. The top and bottom boundaries are assumed to be streamlines and the numerical boundary conditions specified there are $v = 0$ and $\partial q/\partial y = 0$, where $q$ is $\rho, u$, or $p$. Characteristic-based boundary conditions are enforced at the inflow and outflow boundaries in compressible flows. At the entrance, both mass and energy fluxes are kept constant with $v = 0$ specified for the subsonic inflow since there are three incoming characteristics and one outgoing characteristic. For the case of the supersonic inflow, the primitive variables are specified since there are four incoming characteristics. At the exit plane, there are four outgoing characteristics as the exit flow is supersonic and the outflow boundary conditions need not be specified. For the subsonic exit flow, the pressure needs to be specified at the outflow plane since there are three outgoing characteristics and one incoming characteristic. The specification of the initial conditions is based on the experiments.[6,7]

## Results and Discussion

The presentation and discussion of the computational results are classified into three parts: code validation, effects of compressibility,

and mixing enhancement in supersonic shear layers. In all velocity regimes, the density, velocity, and pressure ratios of the two streams are fixed at the same values.

### Code Validation

In one case of the previous experiments,[6,7] the mixing layer is formed by two airstreams at the density ratio $\rho_2/\rho_1 = 0.64$, velocity ratio $\bar{u}_2/\bar{u}_1 = 0.36$, and pressure ratio $p_2/p_1 = 1$. The two free-stream Mach numbers are $M_1 = 1.83$ and $M_2 = 0.51$ and $M_c$ is 0.51. These experimental conditions of a supersonic/subsonic shear layer are used as an initial input of the present calculations for code validation. For this experimental case, a detailed description of the mean flow measurements was given in Samimy and Elliott[6] and the turbulence quantities in Elliott and Samimy.[7] Their measurements[6,7] were performed in the region of $x \leq 21$ cm, before the expansion or compression waves generated at the trailing edge of the splitter plate reflect off the top wall and interact with the shear layer; therefore, the present computational domain is assumed to be 60 cm long and 30 cm high to avoid the reflected waves impinging on the shear layer before $x = 21$ cm. Four sets of uniform grids—202 × 102, 322 × 162, 402 × 202, and 482 × 242 ($x \times y$)—were examined for a grid-independence study and the grid independence was attained for grid sizes of 402 × 202 and 482 × 242. The deviations in the axial mean velocity and turbulence quantities calculated from these two grid systems were approximately negligible (less than 3%). Consequently, the results presented later are based on the 402 × 202 grid system. The Courant number ($a\Delta t/\Delta x$) was fixed at 0.6 to guarantee numerical stability and to advance the code in time properly. All simulations were carried out on a DEC 3000 model 600 workstation, and for this case ($M_c = 0.51$), a complete run for the statistical data obtained by taking a time average over an appropriate period of time ($4 \leq t^* \leq 8$) required about 22 h of CPU time. Although the present numerical method solves the Euler equations directly without SGS turbulence models, numerical dissipation (which has no relation to the laminar viscous terms in a direct simulation) has been considered as a SGS model in many other investigations.[24–27] Especially, Oran and Boris[27] have performed various tests to support that the local, time-dependent numerical dissipation in the Euler equations behaves as a subgrid turbulence model for scales smaller than grid sizes and this subgrid model properly connects the large, energy-containing scales with the unresolved subgrid scales of motion. In fact, the numerical dissipation is here proportional to $\Delta^2$($\Delta$ being the computational

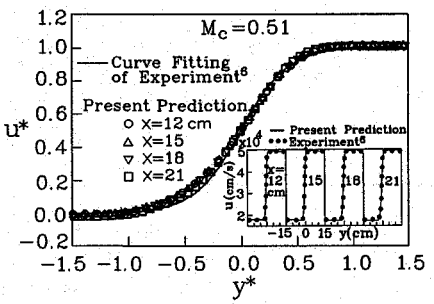


**Fig. 2 Comparison of computed axial mean velocity profiles with measured data for supersonic/subsonic free shear layer.**

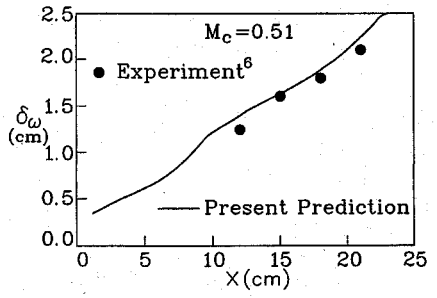


**Fig. 3 Comparison of computed vorticity thickness with measured data for supersonic/subsonic free shear layer.**

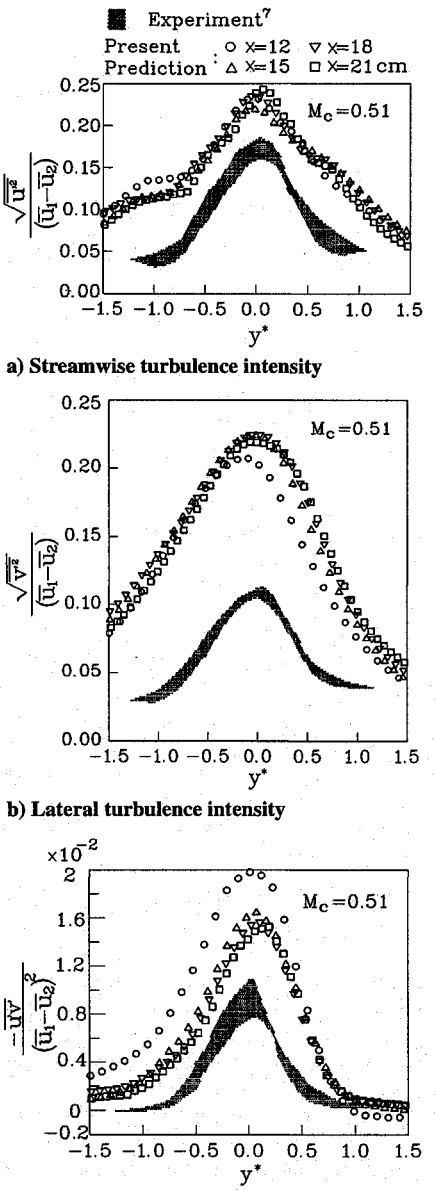


**Fig. 4 Comparison of computed turbulence quantities with measured data for supersonic/subsonic free shear layer.**

resolution), which is very similar to a normal SGS model of dissipative nature.[28]

The calculated results depicted in Figs. 2–4 are the axial mean velocity profiles, axial variation of the vorticity thickness, and distributions of the turbulence quantities, respectively. Experimental data[6,7] are also included for comparison. The variables used in these figures, such as $u^* = (\bar{u} - \bar{u}_2)/(\bar{u}_1 - \bar{u}_2)$, $y^* = (y - y_0)/\delta_w$, and $\delta_\omega = (\bar{u}_1 + \bar{u}_2)/(\partial\bar{u}/\partial y)_{\max}$, are defined as in the experiments. The lateral distributions of the normalized axial mean velocity at various streamwise stations shown in Fig. 2 suggest that the flow attains self-similarity for $x \geq 12$ cm; this feature agrees closely with the experimental results.[6] In addition, the plot of axial mean velocity profiles using the overall physical scales ($u$ vs $y$) is included in Fig. 2 as an inset, which shows that the computed velocity profiles of the physical scales also capture the experimental results satisfactorily. A comparison of the calculated vorticity thickness with the experimental data[6] shown in Fig. 3 indicates that the shear layer growth is predicted reasonably accurately by the present numerical method. A further comparison of the calculated results and experimental data[7] is shown in Figs. 4a–4c in terms of the development of the streamwise and lateral turbulence intensities, and the Reynolds stress ($\sigma_u$, $\sigma_v$, and $-\overline{u'v'}$), respectively. From Fig. 4, one can readily see the following. First, the profiles of the computed turbulence

quantities appear to collapse only for $x \geq 15$ cm, which shows that the turbulence similarity is achieved further downstream than the mean flow similarity. This qualitative feature of the calculated turbulence results is in good accord with the experimental observation.[7] Second, the distribution of the turbulence quantities has a characteristic bell shape, as shown in both calculated and experimental results. The preceding results reveal that the self-similarity feature and bell-shaped curve of the turbulence quantities are still present in the mixing layer of a supersonic/subsonic velocity regime. Third, the calculated turbulence quantities are larger than the experimental data. In this study, the overpredictions are typically within 40% of $\sigma_u$, 90% of $\sigma_v$, and 94% of $-\overline{u'v'}$, as compared with 86% of $\sigma_u$, 56% of $\sigma_v$, and 96% of $-\overline{u'v'}$ in the work of Inoue.[29] In general, the overprediction in the turbulence quantities is a distinctive feature of the two-dimensional numerical simulations in turbulent free shear flows.[29] Nevertheless, the sum of the turbulence intensity peak obtained by a two-dimensional computation seems to be conserved and equal to that of a three-dimensional mixing layer, as indicated by the results of Inoue.[29] Of course, a three-dimensional numerical simulation would be preferred; unfortunately, it is beyond our present computer capability. In sum, from the preceding discussion the calculated results and the corresponding measured data are found to be in good agreement for the mean flow profiles and shear layer growth and generate the same trend for the turbulence parameters. This fact lends reasonable confidence for the present numerical method and following study of the compressibility effects and mixing enhancement in turbulent free shear layers.

**Effects of Compressibility**

Figures 5a–5e show the instantaneous vorticity contours at $t^* = 8$ for various velocity regimes corresponding to different convective Mach numbers, $M_c = 0.14, 0.51, 0.64, 0.86$, and 1.28, respectively. In all cases, the density, velocity, and pressure ratios remain the same as in the case of $M_c = 0.51$ discussed earlier. The main differences in this sequence are that the vortex roll-up in the shear layer appears to be delayed and the large-scale structures are more flattened, elongated, and less mixed as $M_c$ goes up. The snapshot for the subsonic/subsonic velocity regime of low $M_c$ (Fig. 5a) clearly shows the vortex roll-up and pairing process between two adjacent vortices, as is expected from incompressible results.[1,2,10,15] For the cases of supersonic/subsonic velocity regimes (Figs. 5b–5d), a slower development of the shear layers is observed with increasing $M_c$; however, a well-developed vortex roll-up similar to the characteristic of subsonic/subsonic shear layers finally occurs and then the large-scale structures appear in the downstream region, even if one stream of the mixing layer is supersonic and $M_c$ goes up to 0.86. The supersonic/supersonic case (Fig. 5e) exhibits a considerably different behavior, for which vortex roll-up is not observed and the large-scale organized structures are apparently no longer present.

To understand the physics underlying the change in the mixing layer flow structures at high $M_c$, it is useful to study the mechanisms of vorticity dynamics. The vorticity equation for an inviscid, two-dimensional flow can be expressed as

$$\frac{\partial \omega}{\partial t} = -\left(u\frac{\partial \omega}{\partial x} + v\frac{\partial \omega}{\partial y}\right) - \omega\left(\frac{\partial u}{\partial x} + \frac{\partial v}{\partial y}\right) + \frac{1}{\rho^2}\left(\frac{\partial p}{\partial x}\frac{\partial \rho}{\partial y} - \frac{\partial p}{\partial y}\frac{\partial \rho}{\partial x}\right) \tag{4}$$

which states that the rate of change of vorticity is due to three effects (convection, dilatation, and baroclinic torque) corresponding to the terms on the right-hand side of Eq. (4). The cross-sectional averaged magnitudes of these quantities along the streamwise axis are depicted in Figs. 6a and 6b for the cases of $M_c = 0.14$ and 1.28, respectively. It is found that the convection effect is dominant and the dilatation and baroclinic-torque terms are much smaller and almost negligible for the case of $M_c = 0.14$; therefore, the roller-type vortices formed at the trailing edge of the splitter plate will convect downstream and merge with each other to develop a large-scale organized structure in the downstream region as shown in Fig. 5a. However, this feature is changed for the case of $M_c = 1.28$ since a significant dilatation effect appears in this flow, even if the

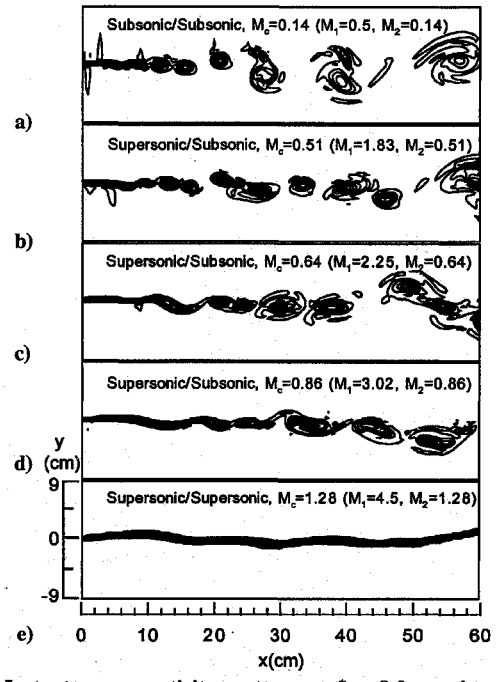


**Fig. 5 Instantaneous vorticity contours at $t^* = 8$ for various velocity regimes.**

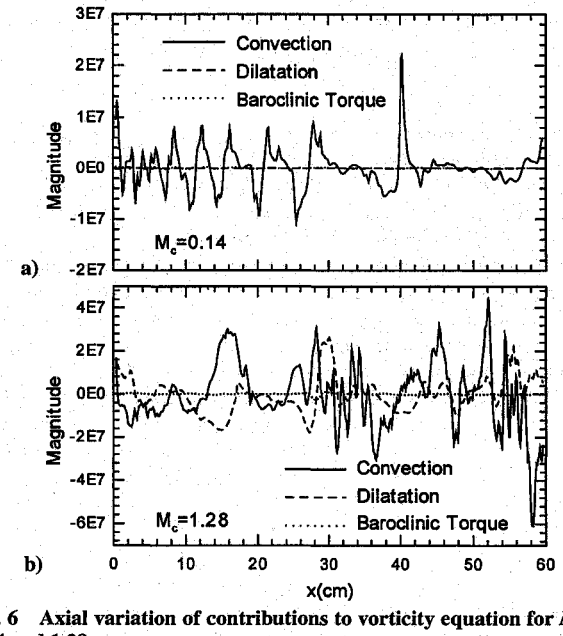


**Fig. 6 Axial variation of contributions to vorticity equation for $M_c$ = 0.14 and 1.28.**

baroclinic-torque effect is still negligible. The dilatation effect is essentially of opposite sign to the convection term (Fig. 6b), and thus it obstructs the development of the vortices (Fig. 5e). In general, the vortex becomes more flattened and elongated in the streamwise direction with increasing $M_c$ (Fig. 5) because the fluid element expands due to the compressibility effects associated with the larger dilatation term. It is also interesting to mention that the physical mechanism responsible for the delay of the vortex roll-up and the change of large-scale structures in subsonic reacting flows results from the significant baroclinic-torque effect associated with heat release, as described in the work of Liou et al.[15] This fact reveals that the compressibility effects on the fluid motions behave in a comparatively different manner as the mechanisms of vorticity dynamics change.

Bogdanoff[3] and Papamoschou and Roshko[5] introduced $M_c$ as a parameter to characterize the intrinsic compressibility effects and quantified the compressibility effects on the growth rate. Their results showed a good correlation between $M_c$ and compressible free shear layer growth rates nondimensionalized by the incompressible shear layer growth rate under the same density and velocity ratios.

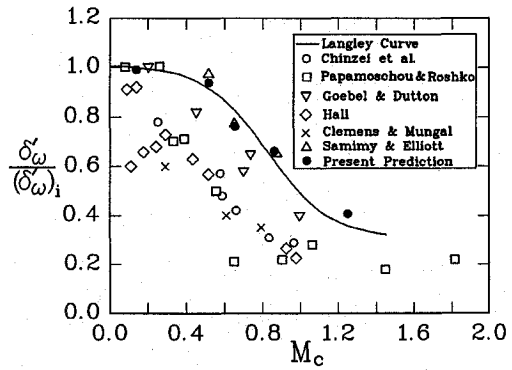


**Fig. 7 Variation of normalized vorticity growth rate with $M_c$.**

Figure 7 compares the calculations of normalized vorticity growth rates with the data shown in Lele's review article,[8] where $(\delta'_\omega)_i = 0.181(\bar{u}_1 - \bar{u}_2)/(\bar{u}_1 + \bar{u}_2)$ used in the present simulations is defined as in the experiment.[6] As can be seen, the calculated results agree very well with the measurements.[6] In addition, Fig. 7 shows a rapid reduction in growth rate as $M_c$ increases from 0.4, resulting from the more elongated vortex structures for higher values of $M_c$, as shown in Fig. 5. The elongated vortex cannot entrain as much fluid as the near-circular vortex structure appearing in the incompressible shear layers; hence, the growth rate of the mixing layer is decreased. The collapse of the normalized mixing layer growth rate data collected in Fig. 7 has significant scatter, which may result from the sensitivity of the mixing layer flow to background disturbance environment, the variable degree of realization to the self-preserving feature, and uncertainty in the normalizing incompressible mixing layer growth rate encountered in different experiments, as addressed by Lele.[8]

### Mixing Enhancement

Faced with the decrease in growth rate of the mixing layer with increasing $M_c$, one important objective of supersonic shear layer research is to devise methods of increasing the mixing between the two streams since, for example, the enhancement in mixing implies the improvement of the performance in supersonic combustion engines. The subsonic shear layer growth rate was demonstrated experimentally to be altered markedly by introducing external perturbations near the point of initial mixing[30,31] and it is interesting to examine whether the same concepts are still effective for achieving the mixing enhancement in supersonic shear layers. Figure 8 shows the instantaneous vorticity contours at $t^* = 8$ for the supersonic/subsonic mixing layer ($M_c = 0.64$) under a sinusoidal normal velocity disturbance at the inflow boundary, which includes various forms of forcings applied at the fundamental frequency ($f_0$) and its first two subharmonics ($f_1$ and $f_2$), each with an amplitude of $0.15(\bar{u}_1 + \bar{u}_2)/2$. The fundamental frequency is obtained from the experimental power spectra of pressure fluctuations[32] that showed a characteristic frequency (5 kHz) of the shear layer near the splitting plate. The evolution of the forced mixing layers is distinctly different from each other and from that of the unforced case (Fig. 5c). When the mixing layer is forced by the fundamental frequency (Fig. 8a), the initial formation of vortices develops quickly and then the vortex merging is suppressed for quite a long distance, i.e., the shear layer in this region consists of a row of well-aligned vortices that do not interact with one another. Eventually, the vortex pairing resumes further downstream as in the unforced mixing layer. For the first subharmonic frequency forcing (Fig. 8b), the vortex-merging suppression occurs later in space. Forcing at the second subharmonic frequency, the merging of three vortices is observed near $x = 30$ cm (Fig. 8c). From the preceding results, the forcing frequency of the normal velocity disturbance is found to have pronounced effects on the evolution of the large-scale structures, even for the supersonic/subsonic mixing layer; in turn, it can effectively manipulate the spreading rate of the mixing layer.

Perhaps a better physical representative of the local width of the mixing layer is provided by the momentum thickness defined as[6]

$$\theta = \int_{-\infty}^{\infty} \frac{\rho}{\rho_1} u^*(1 - u^*)\,dy \qquad (5)$$

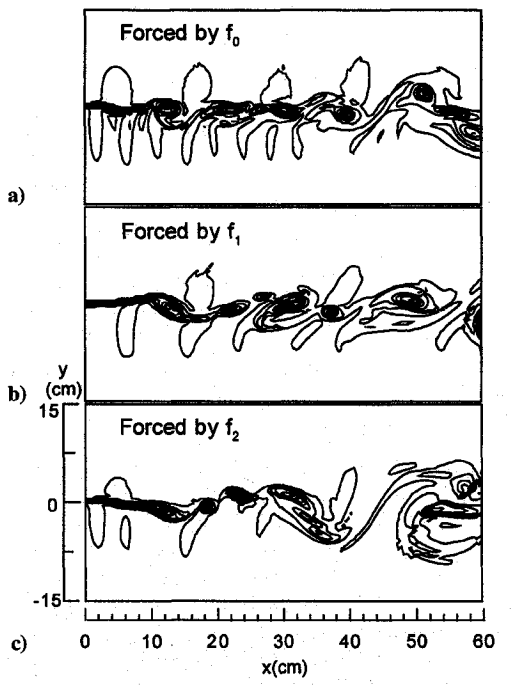


**Fig. 8 Instantaneous vorticity contours at $t^* = 8$ for $M_c = 0.64$ with various types of forcings.**

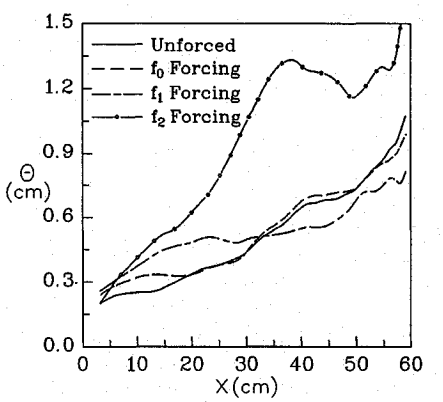


**Fig. 9 Axial variation of momentum thickness for $M_c = 0.64$ with various types of forcings.**

The momentum thickness growth rate is closely related to the shear layer entrainment and spreading rate.[6,30,31] The effect of various types of forcings on the streamwise development of $\theta$ is presented in Fig. 9 for the case shown in Fig. 8. Figure 9 shows that the forcing frequency influences the evolution of $\theta$ markedly as compared with the unforced mixing layer. The streamwise variations of $\theta$ in all forced mixing layers reveal a general tendency characterized by three regions. In region 1, the initial thickness of the forced mixing layer exceeds that of the unforced case. In region 2, the growth rate with increasing $x$ slows down or stops and may even become negative. It is believed that the growth rate is retarded because the large-eddy amalgamations are inhibited, i.e., there are no vortex pairings in region 2, as shown in Fig. 8. Beyond region 2, the mixing layer resumes its downstream growth in region 3. A careful examination of the results in Fig. 9 shows that the length of region 1 appears to be inversely proportional to the forcing frequency. From Figs. 8 and 9, the effects of the forcing frequency on the vortex dynamics and momentum thickness of a supersonic/subsonic mixing layer exhibit a development similar to the experimental observations of subsonic/subsonic mixing layers.[30,31] In addition, the momentum thickness at the end of region 1 for the second subharmonic frequency forcing shown in Fig. 9 is 120% larger than the corresponding unforced flow; consequently, this method of enhancing the mixing in a supersonic/subsonic shear layer may offer an opportunity of improving the performance in the related engineering applications.

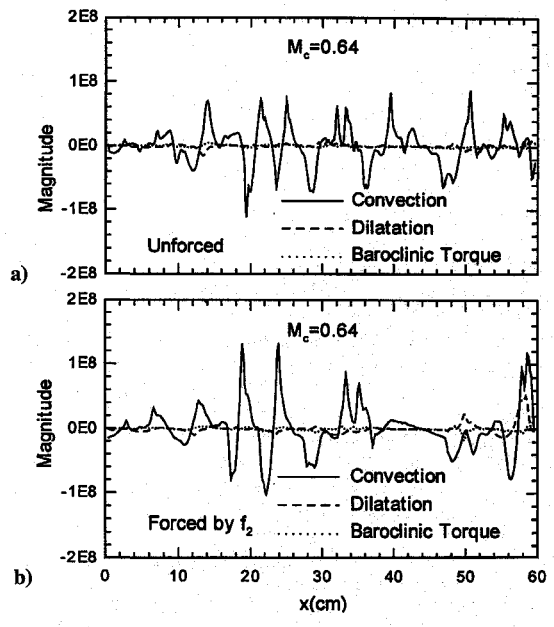


Fig. 10 Axial variation of contributions to vorticity equation for unforced and forced flows.

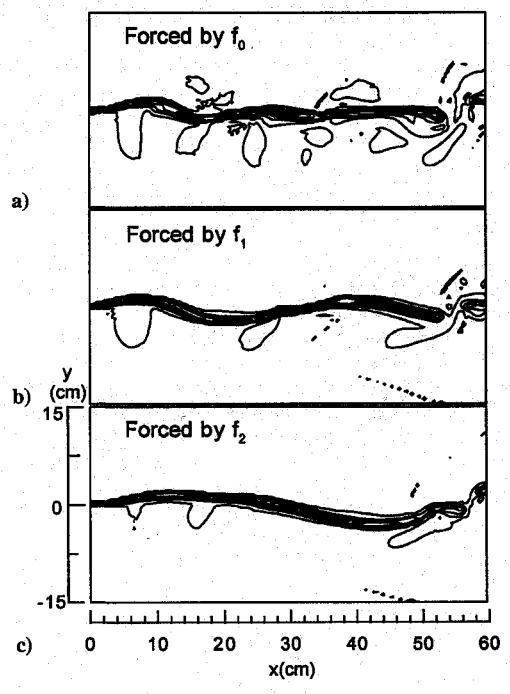


Fig. 11 Instantaneous vorticity contours at $t^* = 8$ for $M_c = 1.28$ with various types of forcings.

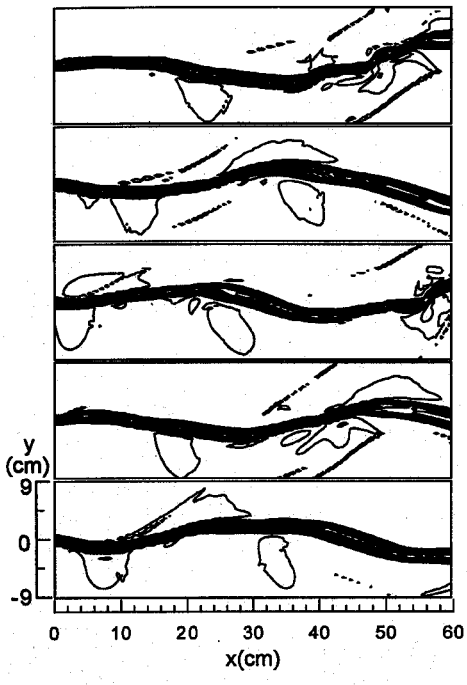


Fig. 12 Time sequence of instantaneous vorticity contours for $M_c = 1.28$ under the second subharmonic frequency forcing, $\Delta t^* = 0.5$.

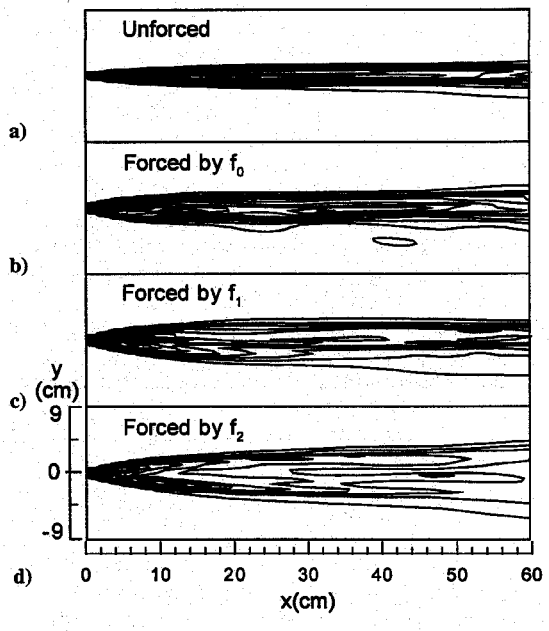


Fig. 13 Time-averaged vorticity contours for $M_c = 1.28$ with various types of forcings.

As for the cause of the mixing enhancement, examining the axial variations of the contributions to the rate of change of vorticity [Eq. (4)] may provide a clear physical rationale. A comparison between the unforced and forced (the second subharmonic frequency forcing) flows is therefore made in Fig. 10. The convection term of the forced flow becomes much larger than the corresponding unforced case, especially in the region between $x = 20$ and 35 cm, whereas the effects of forcing on the dilatation and baroclinic-torque terms appear to be negligible. The augmented convection effect accelerates the vortical motion and makes the vortices merge with each other quickly (Fig. 8c); therefore, the mixing layer grows rapidly (Fig. 9). Lele[33] showed the contours of individual terms of the vorticity equation for one case ($M_c = 0.4$) to describe the stabilizing effect of the dilatation term. The present paper uses the vorticity dynamics analysis to explore the flow mechanisms for different $M_c$ flows and the physics of the mixing enhancement under excitations.

In addition, the axial variations of the cross-sectional averaged magnitudes of various terms on vortex dynamics used in the present study offer a clear understanding of the streamwise evolution of large-scale structures under various $M_c$ and forcing conditions for the first time.

The effects of the normal velocity disturbance on the vortex dynamics of a supersonic/supersonic mixing layer ($M_c = 1.28$) are presented in Fig. 11. The forced mixing layers of the supersonic/supersonic velocity regime reveal a more oscillatory fashion as compared with the unforced case (Fig. 5e). To further visualize the temporal evolution of the forced supersonic/supersonic mixing layers, a time sequence of the instantaneous vorticity contours is shown in Fig. 12 for the case of the second subharmonic frequency forcing. The normalized time interval, $\Delta t^* = \Delta[t/(L/\bar{u}_a)]$, between the two consecutive pictures is 0.5 and the upper one is recorded earlier. These snapshots indicate that the forced supersonic/supersonic mixing layers move up and down with time. By

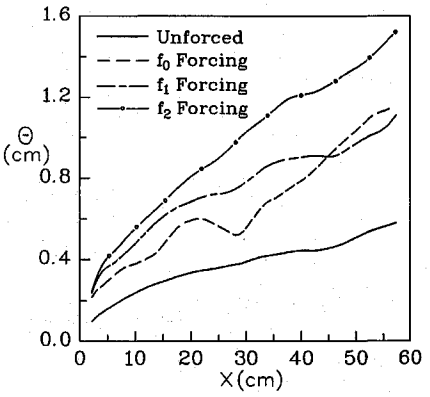


**Fig. 14 Axial variation of momentum thickness for $M_c$ = 1.28 with various types of forcings.**

way of swaying, these oscillatory mixing layers attain a significantly greater rate of growth, as shown in Figs. 13 and 14 that compare the time-averaged vorticity contours and momentum thickness of the forced cases with those of unforced flows, respectively. The mixing enhancement mechanism of supersonic/supersonic mixing layers presents a marked difference from the conventional enhancement mechanism for the subsonic/subsonic mixing layer growth. Quantitatively, the forcing of $f_2$ in the supersonic/supersonic mixing layer can achieve a linear growth rate of 250% of the unforced flow.

## Conclusions

A numerical experiment of two-dimensional turbulent free mixing layers consisting of two coflowing fluid streams under various velocity regimes (subsonic/subsonic, supersonic/subsonic, and supersonic/supersonic) has been performed using an unsteady numerical simulation incorporated with a modified Godunov's scheme. Reasonable agreement between the predicted and available experimental results has been demonstrated. The numerical flow visualization of the vorticity field and the associated vorticity dynamics analysis facilitate a systematic understanding of the streamwise evolution of flow structures under various convective Mach numbers, for instance, providing a rationale for the presence or absence of the vortex roll-up and pairing, and hence for the growth rate of free mixing layers under different degrees of compressibility.

New information is provided that the mixing enhancement for the case of supersonic/supersonic free mixing layers can be achieved as the forced shear layers move up and down with time, a brand new mixing enhancement mechanism in contrast to the conventional vortex roll-up and pairing process for the subsonic/subsonic mixing layers. The present computation also supplements information to the lacking literature for the supersonic/subsonic mixing layers whose growth rate, as reported in this paper, can be significantly enhanced by transversely disturbing the inlet flow with the second subharmonic forcing frequency. A detailed quantitative comparison between the present computation and previous measured data for the supersonic/subsonic mixing layers is reported here for the first time.

## Acknowledgment

The research was supported by the National Science Council of the Republic of China under Contract CS 81-0210-D-007-1003.

## References

[1]Winant, C. D., and Browand, F. K., "Vortex Pairing: The Mechanism of Turbulent Mixing-Layer Growth at Moderate Reynolds Number," *Journal of Fluid Mechanics*, Vol. 63, April 1974, pp. 237–255.

[2]Brown, G. L., and Roshko, A., "On Density Effects and Large Structures in Turbulent Mixing Layers," *Journal of Fluid Mechanics*, Vol. 64, July 1974, pp. 775–816.

[3]Bogdanoff, D. W., "Compressibility Effects in Turbulent Shear Layers," *AIAA Journal*, Vol. 21, No. 6, 1983, pp. 926, 927.

[4]Chinzei, N., Masuya, G., Komuro, T., Murakami, A., and Kudou, K., "Spreading of Two-Stream Supersonic Turbulent Mixing Layers," *Physics of Fluids*, Vol. 29, No. 5, 1986, pp. 1345–1347.

[5]Papamoschou, D., and Roshko, A., "The Compressible Turbulent Shear Layer: An Experimental Study," *Journal of Fluid Mechanics*, Vol. 197, Dec. 1988, pp. 453–477.

[6]Samimy, M., and Elliott, G. S., "Effects of Compressibility on the Characteristics of Free Shear Layers," *AIAA Journal*, Vol. 28, No. 3, 1990, pp. 439–445.

[7]Elliott, G. S., and Samimy, M., "Compressibility Effects in Free Shear Layers," *Physics of Fluids A*, Vol. 2, No. 7, 1990, pp. 1231–1240.

[8]Lele, S. K., "Compressibility Effects on Turbulence," *Annual Review of Fluid Mechanics*, Vol. 26, 1994, pp. 211–254.

[9]Grinstein, F. F., Oran, E. S., and Boris, J. P., "Numerical Simulations of Asymmetric Mixing in Planar Shear Flows," *Journal of Fluid Mechanics*, Vol. 165, April 1986, pp. 201–220.

[10]Lowery, P. S., Reynolds, W. C., and Mansour, N. N., "Passive Scalar Entrainment and Mixing in a Forced, Spatially-Developing Plane Mixing Layer," AIAA Paper 87-0132, Jan. 1987.

[11]Sandham, N. D., and Reynolds, W. C., "Some Inlet-Plane Effects on the Numerically Simulated Spatially-Developing Mixing Layer," *Turbulent Shear Flow 6*, Springer–Verlag, Berlin, 1989, pp. 441–453.

[12]Farouk, B., Oran, E. S., and Kailasanath, K., "Numerical Simulations of the Structure of Supersonic Shear Layers," *Physics of Fluids A*, Vol. 3, No. 11, 1991, pp. 2786–2798.

[13]Lu, P. J., and Wu, K. C., "On the Shock Enhancement of Confined Supersonic Mixing Flows," *Physics of Fluids A*, Vol. 3, No. 12, 1991, pp. 3046–3062.

[14]Lu, P. J., and Wu, K. C., "Numerical Investigation on the Structure of a Confined Supersonic Mixing Layer," *Physics of Fluids A*, Vol. 3, No. 12, 1991, pp. 3063–3079.

[15]Liou, T.-M., Lien, W.-Y., and Hwang, P.-W., "Large-Eddy Simulations of Turbulent Reacting Flows in a Chamber with Gaseous Ethylene Injecting through the Porous Wall," *Combustion and Flame*, Vol. 99, No. 2, 1994, pp. 591–600.

[16]Roshko, A., "Structure of Turbulent Shear Flows: A New Look," *AIAA Journal*, Vol. 14, No. 10, 1976, pp. 1349–1357.

[17]Papamoschou, D., "Structure of the Compressible Turbulent Shear Layer," AIAA Paper 89-0126, Jan. 1989.

[18]Clemens, N. T., and Mungal, M. G., "Two- and Three-Dimensional Effects in the Supersonic Mixing Layer," *AIAA Journal*, Vol. 30, No. 4, 1992, pp. 973–981.

[19]Sandham, N. D., and Reynolds, W. C., "Compressible Mixing Layer: Linear Theory and Direct Simulation," *AIAA Journal*, Vol. 28, No. 4, 1990, pp. 618–624.

[20]Sandham, N. D., and Reynolds, W. C., "Three-Dimensional Simulations of Large Eddies in the Compressible Mixing Layer," *Journal of Fluid Mechanics*, Vol. 224, March 1991, pp. 133–158.

[21]Riley, J. J., and Metcalfe, R. W., "Direct Numerical Simulation of a Perturbed, Turbulent Mixing Layer," AIAA Paper 80-0274, Jan. 1980.

[22]Godunov, S. K., "A Difference Method for Numerical Calculation of Discontinuous Solutions of the Equations of Hydrodynamics," *Mathematics Sbornik*, Vol. 47, No. 3, 1959, pp. 271–306.

[23]Liou, T.-M., Lien, W.-Y., and Hwang, P.-W., "A Modified Godunov's Scheme for Shock Tube Flows and Turbulent Combustion Flows," *The Fourth National Conference on Combustion Science and Technology*, Combustion Inst. of ROC, Hsinchu, Taiwan, ROC, 1994, pp. 242–247.

[24]Jou, W. H., and Riley, J. J., "Progress in Direct Numerical Simulations of Turbulent Reacting Flows," *AIAA Journal*, Vol. 27, No. 11, 1989, pp. 1543–1556.

[25]Kailasanath, K., Gardner, J. H., Boris, J. P., and Oran, E. S., "Numerical Simulations of Acoustic-Vortex Interactions in a Central-Dump Ramjet Combustor," *Journal of Propulsion and Power*, Vol. 3, No. 6, 1987, pp. 525–533.

[26]Kailasanath, K., Gardner, J. H., Boris, J. P., and Oran, E. S., "Acoustic-Vortex Interactions and Low-Frequency Oscillations in Axisymmetric Combustors," *Journal of Propulsion and Power*, Vol. 5, No. 2, 1989, pp. 165–171.

[27]Oran, E. S., and Boris, J. P., "Computing Turbulent Shear Flows—A Convenient Conspiracy," *Computers in Physics*, Vol. 7, No. 5, 1993, pp. 523–533.

[28]Smagorinsky, J., "General Circulation Experiments with the Primitive Equations," *Monthly Weather Review*, Vol. 91, No. 3, 1963, pp. 99–164.

[29]Inoue, O., "Vortex Simulation of a Turbulent Mixing Layer," *AIAA Journal*, Vol. 23, No. 3, 1985, pp. 367–373.

[30]Ho, C. M., and Huang, L. S., "Subharmonics and Vortex Merging in Mixing Layers," *Journal of Fluid Mechanics*, Vol. 119, June 1982, pp. 443–473.

[31]Oster, D., and Wygnanski, I., "The Forced Mixing Layer Between Parallel Streams," *Journal of Fluid Mechanics*, Vol. 123, Oct. 1982, pp. 91–130.

[32]Samimy, M., Reeder, M. F., and Elliott, G. S., "Compressibility Effects on Large Structures in Free Shear Flows," *Physics of Fluids A*, Vol. 4, No. 6, 1992, pp. 1251–1258.

[33]Lele, S. K., "Direct Numerical Simulation of Compressible Free Shear Flows," AIAA Paper 89-0374, Jan. 1989.